

Determination of fracture toughness of thin-film amorphous silicon using spiral crack structures

Torsten Bronger¹

¹*Forschungszentrum Jülich GmbH, Institut für Energie und Klimaforschung (IEK-5), Jülich, 52425 (Germany)*

We prepared thin layers of amorphous silicon by deposition of a liquid-phase polysilane precursor on glass substrate. Raman scattering provides evidence for residual tensile stress in the silicon, which is evaluated quantitatively. Under treatment with hydrofluoric acid, this stress leads to spiral cracks in the silicon. We explain the process of crack formation and examine this phenomenon both analytically and numerically, the latter with the finite element method (FEM). The FEM yields the geometry correction factor for such spiral cracks in terms of the Griffith criterion. This allows for the first time the determination of fracture toughness of amorphous silicon, which is greatly enhanced in comparison with crystalline silicon.

INTRODUCTION

Semiconductor layers made from liquid-phase precursors have gained interest in recent years. On the one hand, they promise low production costs, and on the other hand, device quality could be increased significantly. In particular, as recently reported, the efficiency of solar cells made of liquid silicon precursors reaches 3.5%. [1]

One challenge of this technique is the forming of a low-stress layer. The cause of the residual stress is largely unknown. Possible candidates are the high temperature change as well as the chemical processes during the drying. Stress in thin layers deposited on substrates is a topic of interest due to potential delamination of the layer. Such delamination usually renders the sample or the device unusable. It is caused by interfacial cracking between layer and substrate in case the stress in the layer is large enough. Moreover, stress may induce the formation of voids in the material, and it has been shown to cause defects in amorphous silicon (a-Si:H) [2]. For amorphous silicon prepared by plasma-enhanced chemical vapour deposition, the stress is well-controlled to a point that it usually imposes no problem for the resulting device. However, for other material systems like micro-crystalline silicon, or other fabrication techniques like the deposition from liquid-phase precursors as used in our work, it may limit the achievable thickness or device quality. [1]

For characterising stress in silicon, Raman spectroscopy is a well-established method [3], also in the micro-Raman variant [4]. There exists a linear relationship between in-plane stress and the shift of the Si-Si peaks. [5] In case of a single crystal, this shift may occur in conjunction with a peak split for crystalline material. [5]

Another way for stress to become visible is the generation of cracks. A small initial weakness in the layer may be the origin of a crack propagating and thus relaxing the stressed layer. Theoretically, this phenomenon can be analysed both analytically (important breakthroughs

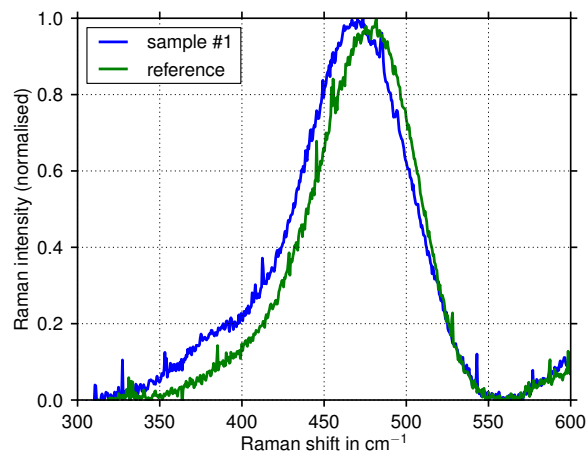


FIG. 1. Raman spectra of the stressed sample #1 and a PECVD a-Si:H reference sample with 700 nm thickness. The laser excitation wavelength is 488 nm.

were the Griffith theory founded in [6] and the introduction of the stress intensity factor in [7]), and numerically by the finite element method FEM [8] and the boundary element method BEM [9].

In this work, we will describe spiral crack formation in etched amorphous silicon layers prepared from a liquid-phase precursor. We will present a model for the development of the cracks. Finally, we will use this model for analysing the observations with an analogy to Griffith's theory as well as with extensive FEM simulations, yielding the fracture toughness of the silicon material.

EXPERIMENTS

The samples are single layers of amorphous silicon, made from soluble polysilane precursor, deposited on glass substrate (Corning Eagle 2000). The thickness of the silicon layer varies between 130 and 190 nm. Figure 1 shows Raman measurements of liquid-phase precursor sample #1 and a PECVD reference sample. Obviously, the peak at 480 cm^{-1} , which is attributed to a-Si:H,

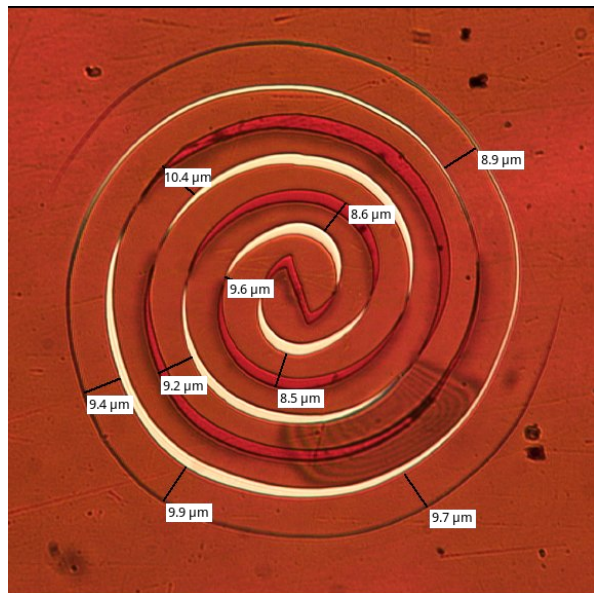


FIG. 2. Transmitted-light microscope image of a crack structure in an a-Si:H layer. Yellow areas denote lack of layer material, i. e. only the substrate is visible. Two material layers on top of each other appear in reddish colour. At various places, the stripe width is measured, and the resulting value is shown.

sample #	Raman peak shift in cm^{-1}	stripe width w in μm
1	-9.1	7.5
2	-9.0	9.5
3	-7.7	10.0
4	-6.5	8.0

TABLE I. Measured shift of the a-Si:H Raman peak and spiral stripe width for a-Si:H samples.

is shifted to smaller wavenumbers for the sample #1. As derived by [10], the hydrostatic in-plane stress σ and change in Raman peak shift $\Delta\omega$ for single-crystal silicon are related linearly:

$$\sigma = -249 \text{ MPa cm} \cdot \Delta\omega. \quad (1)$$

For $\Delta\omega < 0$, this means $\sigma > 0$, i. e. tensile stress. In accordance with [11], we apply eq. (1) to the a-Si:H peak at 480 nm, too.

After the fabrication, the samples were etched in hydrofluoric acid (20%) for approximately 10 seconds. Afterwards, they were carefully blow-dried with nitrogen.

Figure 2 shows microscopic pictures of the samples after etching. As you can see, spiral cracks have been formed. In most cases, they are interleaved double spirals but we also observed single ones. The width w of the spiral stripes is rather constant along the stripe length, and constant on a given sample. Furthermore, the two outer end points of the cracks are in opposite position to

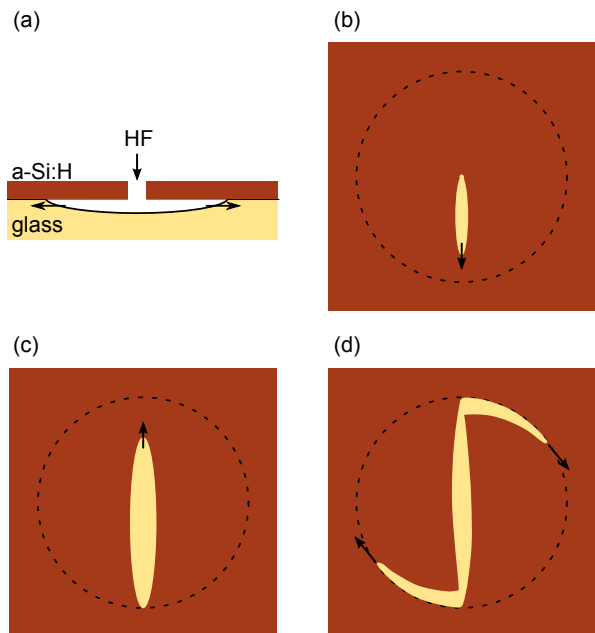


FIG. 3. The crack propagation model for spiral fractures in a-Si:H. (a) is a cross section of the layer structure, (b-d) are top views. The arrows denote the direction of etching (a) or crack propagation (b-d). The dashed circle is the area of underetching. The colours mimic the colours in figure 2.

each other, or very close to that position. We observed no preferred winding direction. Table I lists the Raman peak shifts $\Delta\omega$ and the spiral stripe widths w for the measured samples.

MODEL OF CRACK FORMATION

Figure 3 illustrates how we think these spiral cracks come into existence during etching.

The hydrofluoric acid etches glass very efficiently. In contrast, it leaves silicon more or less unaffected. The acid probably attacks a weakness in the silicon layer, see figure 3 (a). This weakness may be a tiny hole, or a small inclusion of etchable material, e. g. SiO_2 . In any way, the acid penetrates the weakness and starts underetching the silicon. This leads to a disk-shaped zone of underetching with the weakness in the centre. Above this zone, the silicon is unsupported and thus, the stress in the material is no longer sustained by the substrate. In figure 3 (b-d), this zone is marked by the dashed circle.

A small asymmetry of the initial hole, e. g. a notch in its edge, concentrates the stress and begins to crack. The crack tip propagates towards the rim of the underetching, see figure 3 (b). While doing so, the stress intensity factor increases according to $\text{SIF} \sim \sqrt{\text{crack length}}$. Note that this also drastically increases the stress at the initial hole, so that eventually, a second crack forms and grows towards the rim, see figure 3 (c).

Both crack tips eventually reach the rim, one of them first. This one continues on the rim itself, determining the winding direction of the final spiral. The slightly slower crack tip takes the same direction because the shearing stress due to the asymmetrical situation caused by the already cracked rim on the opposite side guides it this way.

Both cracks continue on the rim until the relaxation has reduced the stress so much that no further crack growth is possible, see figure 3 (d). However, at the same time, the underetched disk grows. The newly detached silicon adds new stress to the layer, which lets the cracks start growing again. Both processes happen simultaneously. This way, the spirals are formed. We assume that crack growth is much faster than disk growth, so that the stress intensity factor (SIF) at the crack tips always is very close to the fracture toughness K_{Ic} of the material. In particular, this means that the spiral stripe width is largely independent of the kinematics of the processes, but only dependent on layer properties.

ESTIMATION OF FRACTURE TOUGHNESS

The only quantity easily accessible for measurement is the stripe width of the spiral. Therefore, it is important to understand the mechanism behind it. Apparently, it is a constant for a certain sample, and in particular independent of the distance from the centre of the spiral. A plausible albeit not rigorous explanation is the following:

Figure 4 compares the well-understood Griffith fracture with our geometry. The Griffith fracture occurs in an infinitely large workpiece which contains an initial crack. Additionally, the workpiece is stressed perpendicular to the crack. Then, the stress intensity factor SIF is given by

$$\text{SIF} = \sigma\sqrt{\pi a}f, \quad (2)$$

with σ being the stress in the material, a being the half crack length, and f being the geometry factor, which is unity for the Griffith fracture. f deviate from unity if e. g. the angle between the crack and the stress differs from 90° . It is important to see how the SIF is generated: The lines of force from the length a (shown in red) are deviated to the crack tip because the edges of the crack are load-free.

The right-hand side of figure 4 depicts the situation in the spiral: The arc to the left is the border of the underetching. The crack tip is the join of the lower line coming from the right with the arc. Since the inner (i. e. right) edge of the stripe is load-free, the radial component of the stress vanishes. The circular component, however, is only slightly weakened by the opening of the crack at the bottom.

The characteristic length in this case is the stripe width w . It corresponds to the half crack length in the

Griffith fracture because all lines of force that end in the crack tip pass this width more or less perpendicularly. Moreover, the circular stress decays only slightly towards the inner edge, i. e. in can be assumed homogeneous like for the Griffith fracture.

This suggests that eq. (2) also applies here with $a = w$. Finally, assuming the model of crack formation of the previous section which implies $\text{SIF} = K_{Ic}$, this allows the estimation of fracture toughness according to

$$K_{Ic} = \sigma\sqrt{\pi w}f. \quad (3)$$

This result holds for single and double spirals alike, as long as the process of crack formation, i. e. a slowly growing disk-shaped detachment, is the same. At least after the first winding of the spiral, the local geometry of crack and forces is equivalent in both cases. This is also what is observed experimentally: For both types of spirals, w is the same for a given sample.

The next task is to back this up by accurate simulation, which also helps to determine the particular factor f for the spiral geometry.

FEM SIMULATION

Because the arguments presented in the previous section are non-rigorous, a numerical simulation of the geometry was performed in order to get results on a solid basis. Additionally, such a simulation provides a value for the f geometry factor.

We used the finite element method FEM for this numerical simulation. The FEM is a well-understood and reliable method in fracture mechanics. Moreover, there are plenty of programs and programming libraries that aid developing FEM models. In particular, we chose the SfePy programming library for our research. [12] It is free software, well-documented, and mature. Besides, the Python programming language allows for convenient developing.

We chose a triangular FEM mesh for covering the disk of underetched material, see figure 5. In this mesh, the current crack was realised by severing the nodes along the crack path (duplicating the nodes). Then, the elements at the crack tips were replaced with hundreds of small sub-elements which became even smaller towards the tip. This way, we had the accuracy needed for calculating reliable SIFs.

The SIFs were calculated with the “displacement method”. The displacements of the nodes of the sub-elements (i. e. in a range of one big finite element) were computed into SIF values which were extrapolated for $r \rightarrow 0$, with r being the distance to the tip. We calculated both K_I and K_{II} , and used them for determining the equivalent SIF according to [13] and the crack direction according to [14].

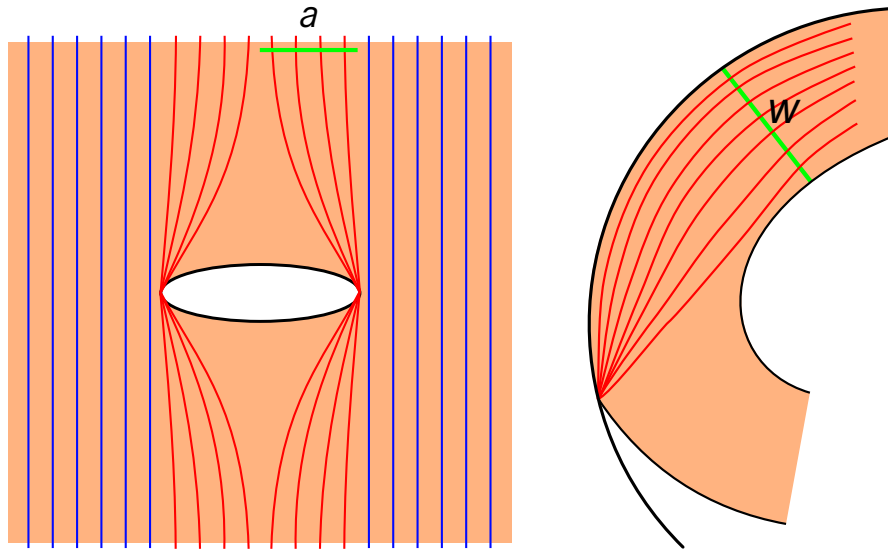


FIG. 4. Comparison of the geometries of the Griffith fracture (left) with the situation in the spirals of the thin-film samples (right). The characteristic crack length is marked in green.

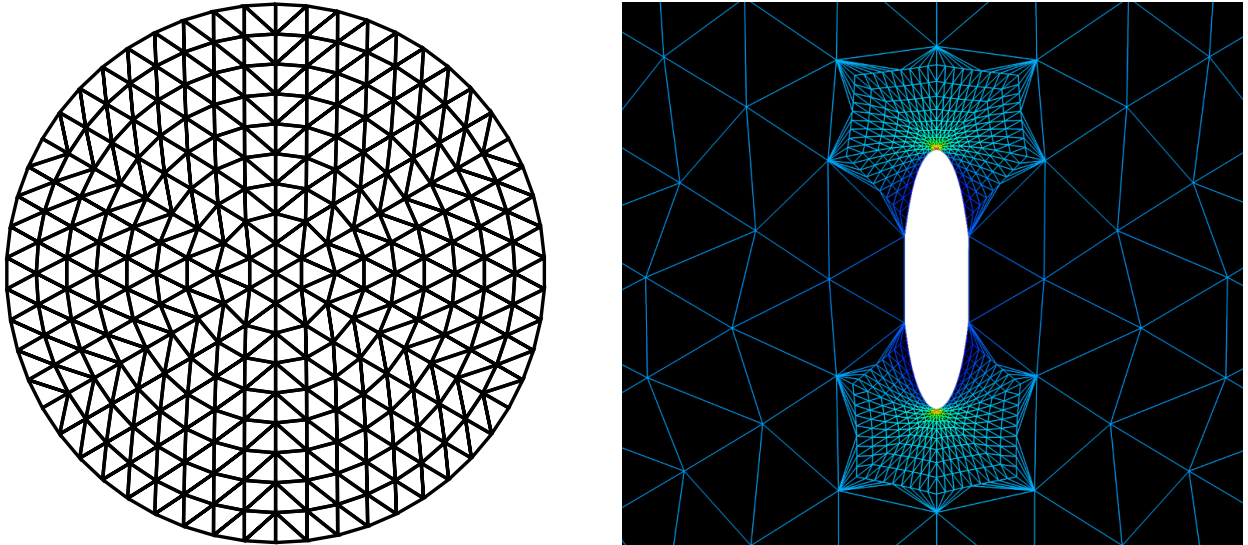


FIG. 5. The triangulation used for the FEM simulations. The triangular mesh for the disk (left), and the additional triangulation for the crack tips (right). On the right-hand side, increasing tension is visualised by the colour sequence blue–cyan–green–yellow–red.

If the equivalent SIF exceeds the fracture toughness of the material, the crack propagates. Then, the crack direction determines which node is the next to be severed. This node is severed, and the new, longer crack has to be analysed by FEM. This is repeated until the material is relaxed enough so that the crack cannot grow anymore.

It is difficult to simulate crack growth without any a priori assumptions because then, you have to crack element after element, which uses a lot of computation time. Also, discretised directions impose inaccuracy to the simulation: Since the polygonal elements have only a certain number of edges originating at each vertex (node), the

calculated crack direction has to be constrained onto one of the edges. This cannot be mitigated by increasing the spatial resolution.

Therefore, we made some preliminary simulations to narrow the degrees of freedom of the crack growth. This showed the following:

1. Any initial crack, originating at the centre of the disk, grows straight towards the rim.
2. Any small deviation from the straight line makes the other tip of the crack deviate in the same direction (e.g. clockwise). In other words, the tips

try to evade each other.

3. When the crack propagates along the rim, its growth direction points outwards. Thus, it must stay on the rim.

Another trivial observation is that a symmetric initial crack (e.g. straight through the centre over the total diameter) conserves symmetry over the whole simulation. This means that only one crack tip has to be analysed, and the other one just mirrors its propagation. These observations confirm the formation model as presented in section .

Hence, the outline of the simplified algorithm is as follows:

1. Create a straight initial crack through the total diameter of the initial disk.
2. Find the length of the crack on the rim of the disk for which the SIF at the tip equals the fracture toughness of the material, and let the crack grow to this length.
3. Add another ring of finite elements around the disk. This brings new stress into the material, and the crack can grow further.
4. If the winding number of the spiral is below a preset value, go back to (2). Otherwise, end the simulation.

Figure 6 presents the result of the FEM in an illustrative manner: The finite elements are displaced according to the values of tension in the spiral lobes. This way, it simulates a top view on the sample. And indeed, this image and the microscopic photograph in figure 2 match very well. The alternation of gap and overlay is properly reproduced, as is the constant stripe width.

Figure 7 analyses the FEM results quantitatively by cutting two perpendicular planes out of the three-dimensional parameter space, namely $\sigma(w)$ and $K_{Ic}(w)$. The two lines correspond to

$$\sigma(w) = \frac{K_{Ic}}{0.44\sqrt{\pi w}} \quad (4)$$

$$K_{Ic}(w) = 0.44\sigma\sqrt{\pi w}. \quad (5)$$

This equation set is compatible with eq. (3). Thus, the FEM confirms the analytical approach of section and yields a value for the geometry factor:

$$K_{Ic}^{\text{spiral}} = \sigma\sqrt{\pi w}f, \quad f = 0.44 \quad (6)$$

APPLICATION TO THE EXPERIMENTS AND DISCUSSION

Applying eq. (1) to the results of table I and then using eq. (6) yields the fracture toughness of each sample. The

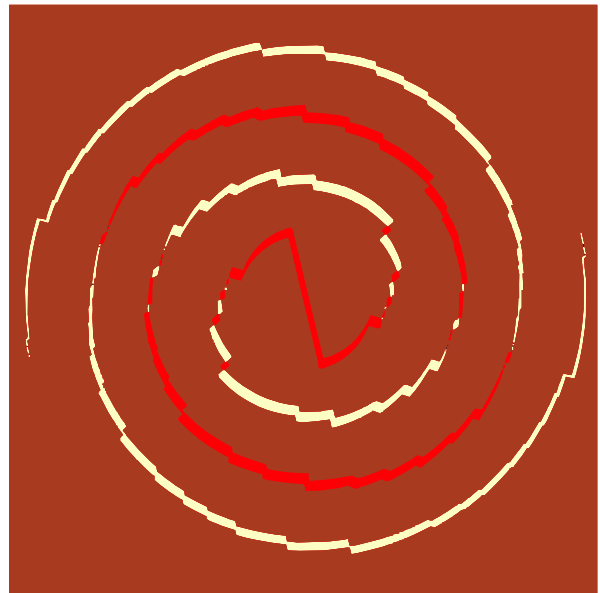


FIG. 6. Visualisation of displacement as a result of an FEM simulation of crack growth in a layer with disk-shaped detachment from the substrate. You can see the spiral lobes being moved out of their original position due to stress forces. The layer is brown, the substrate yellow, and two lobes of the layer stacked on top of each other are red. These colours are chosen to match the colours of figure 2.

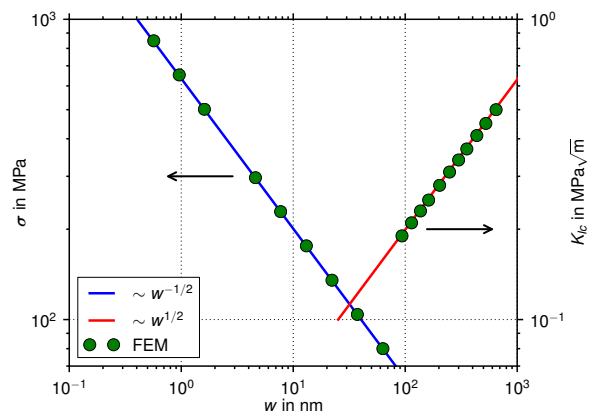


FIG. 7. Disk tension σ and fracture toughness K_{Ic} for various spiral stripe widths w , as determined with FEM simulations. The assumed fracture toughness for the σ curve is $K_{Ic} = 0.5 \text{ MPa}\sqrt{\text{m}}$. The tension in the layer for the K_{Ic} curve is 800 MPa . The lines indicate a fit with eq. (3) and $f = 0.44$.

averaged fracture toughness of the amorphous silicon in the samples is

$$K_{Ic}^{\text{a-Si:H}} = 4.7(3) \text{ MPa}\sqrt{\text{m}}. \quad (7)$$

This value should be compared with the K_{Ic} of single-crystal silicon of $0.82 \text{ MPa}\sqrt{\text{m}}$ [15] and that of polycrystalline silicon in the range $0.86\text{--}1.1 \text{ MPa}\sqrt{\text{m}}$ [16–18]. [19] reports a lower limit of K_{Ic} of a-Si:H at $1.35 \text{ MPa}\sqrt{\text{m}}$. It has been frequently reported (e.g. by [19, 20]) that

amorphous phases exceed their crystalline counterparts in fracture toughness, sometimes by more than a decade. Thus, we consider the above $K_{Ic}^{a-Si:H}$ in plausible accordance with previous findings.

We consider the variation of the measured stripe widths the dominating error in the result. Therefore, we used this as the standard error of the mean in eq. (7). Other contributing errors are the difference between a-Si:H and c-Si with respect to eq. (1) and the uncertainty in the Raman peak shift.

CONCLUSIONS

Thin layers of amorphous silicon from a liquid-phase polysilane precursor may suffer from high residual tensile stress. By underetching the layer through a pinhole, cracks in form of single and double spirals are forming due to this stress. By making an analogy between the spiral cracks and the Griffith fracture, one can identify the spiral stripe width with Griffith's crack length. An analysis with the FEM confirms this analogy and yields the geometry factor for such spirals $f_{\text{spiral}} = 0.44$. The spiral stripe width depends only on stress and fracture toughness, i. e. knowing one leads to the other. We determined the stress by Raman measurements, thus being able to calculate the fracture toughness of the amorphous silicon $K_{Ic}^{a-Si:H} = 4.7 \text{ MPa}\sqrt{\text{m}}$ with a standard error of 8%. This value exceeds that of crystalline silicon by a factor of 5.7.

Further investigation is necessary. The independence of fracture toughness and stress should be confirmed. For this, samples covering a range of stress intensities should be examined, and verified that $\sigma \sim 1/\sqrt{w}$ for all of them. Moreover, eq. (1) should be calibrated for a-Si:H using a direct method like a bendable substrate. Finally, pinholes may be created in the layer deliberately, trying to use the spiral cracks as a very simple albeit destructive method to determine fracture toughness for various types of thin-layer material. This way, fracture toughness may become an additional useful characterisation quantity for such layers.

-
- [1] T. Bronger, P. H. Wöbkenberg, J. Wördenweber, S. Muthmann, U. W. Paetzold, V. Smirnov, S. Traut, Ü. Dagkaldiran, S. Wieber, M. Cölle, *et al.*, Solution-based silicon in thin-film solar cells, *Advanced Energy Materials* (2014).
 - [2] M. Stutzmann, Role of mechanical stress in the light-induced degradation of hydrogenated amorphous silicon, *Applied Physics Letters* **47**, 21 (1985).
 - [3] E. Anastassakis, A. Pinczuk, E. Burstein, F. Pollak, and

- M. Cardona, Effect of static uniaxial stress on the raman spectrum of silicon, *solid state Communications* **8**, 133 (1970).
- [4] I. De Wolf, Micro-Raman spectroscopy to study local mechanical stress in silicon integrated circuits, *Semiconductor Science and Technology* **11**, 139 (1996).
- [5] E. Anastassakis, A. Cantarero, and M. Cardona, Piez-Raman measurements and anharmonic parameters in silicon and diamond, *Physical Review B* **41**, 7529 (1990).
- [6] A. Griffith, Vi. the phenomena of rupture and flow in solids., *Phil. Trans. Roy. Soc. (Lon.) A* **221**, 163 (1920).
- [7] G. R. Irwin, Analysis of stresses and strains near the end of a crack traversing a plate, *J. appl. Mech.* (1957).
- [8] S. Chan, I. Tuba, and W. Wilson, On the finite element method in linear fracture mechanics, *Engineering Fracture Mechanics* **2**, 1 (1970).
- [9] G. E. Blandford, A. R. Ingraffea, and J. A. Liggett, Two-dimensional stress intensity factor computations using the boundary element method, *International Journal for Numerical Methods in Engineering* **17**, 387 (1981).
- [10] E. Anastassakis, Physical problems in microelectronics, *Proceedings of the 4th International School ISPPM, Varna, Bulgaria*, 128 (1985).
- [11] J. Ge, R. Stangl, A. AG, and T. Mueller, Detailed micro Raman spectroscopy analysis of doped silicon thin film layers and its feasibility for heterojunction silicon wafer solar cells, *Journal of Materials Science and Chemical Engineering* **2013** (2013).
- [12] R. Cimrman *et al.*, SfePy: Simple finite elements in python (2008).
- [13] H. Richard, M. Fulland, and M. Sander, Theoretical crack path prediction, *Fatigue & Fracture of Engineering Materials & Structures* **28**, 3 (2005).
- [14] A. M. Alshoaibi and A. K. Ariffin, Finite element simulation of stress intensity factors in elastic-plastic crack growth, *Journal of Zhejiang University Science A* **7**, 1336 (2006).
- [15] L. L. Mercado, H. Wieser, and T. Hauck, Multichip package delamination and die fracture analysis, *Advanced Packaging, IEEE Transactions on* **26**, 152 (2003).
- [16] I. Chasiotis, S. Cho, and K. Jonnalagadda, Fracture toughness and subcritical crack growth in polycrystalline silicon, *Journal of applied mechanics* **73**, 714 (2006).
- [17] J. Bagdahn, J. Schischka, M. Petzold, and W. N. Sharpe Jr, Fracture toughness and fatigue investigations of polycrystalline silicon, in *Micromachining and Micro-fabrication* (International Society for Optics and Photonics, 2001) pp. 159–168.
- [18] H. Kahn, N. Tayebi, R. Ballarini, R. Mullen, and A. Heuer, Fracture toughness of polysilicon mems devices, *Sensors and Actuators A: Physical* **82**, 274 (2000).
- [19] J. G. Swadener and M. Nastasi, Increasing the fracture toughness of silicon by ion implantation, *Nuclear Instruments and Methods in Physics Research Section B: Beam Interactions with Materials and Atoms* **206**, 937 (2003).
- [20] C. Gilbert, J. R. Ritchie, and W. Johnson, Fracture toughness and fatigue-crack propagation in a zr-ti-ni-cu-be bulk metallic glass, *Applied Physics Letters* **71**, 476 (1997).